Progress In Electromagnetics Research, PIER 59, 17–38, 2006

DEVELOPMENT OF A 10 GHZ PHASED ARRAY CYLINDRICAL ANTENNA SYSTEM INCORPORATING IF PHASE PROCESSING

N. C. Athanasopoulos and N. K. Uzunoglu

Microwaves & Fiber Optics Laboratory
National Technical University of Athens
9 Iroon Polytechneiou str. 15780, Athens, Greece

J. D. Kanellopoulos

National Technical University of Athens
9 Iroon Polytechneiou str. 15780, Athens, Greece

Abstract—This paper presents an experimental Phased Array Antenna System operating at 10 GHz. Geometry of the antenna array is cylindrical. Antenna element excitation phases are adjusted at the intermediate frequency stage. Antenna element excitation amplitudes are taken to be constant. A least squares technique is used for phase computation and radiation pattern synthesis. The obtained radiation patterns provide steerable main lobes and nulls at predefined directions including control of the side lobes at specified levels. Units of the system are presented in detail and their architecture is explained. A phase calibration is used to compensate the system. Measurements of radiation patterns are presented and are compared with calculated patterns.

1. INTRODUCTION

The idea of developing antenna array systems with electronically controlled beams has been proposed as early as 1940's [1–4]. Despite this fact, the realization of phased array antenna systems was delayed for many decades, mainly because of the very high development and maintenance costs. Recently, with the advances in microwave monolithic integrated circuits (MMIC) technology, phased array antenna systems have started to become feasible at a reasonable cost.

It has been shown that the use of phased array technologies could provide significant improvement compared to conventional mechanically steering antennas, with the most important benefits being [5]:

- Absence of mechanical movements in antenna systems.
- Fast search of a given field of view.
- Simultaneous tracking of many targets.
- Interference suppression capability.
- Flexible control of radiation patterns such as polarization and side lobe levels.

Many beamforming techniques, based on amplitude and phase control or phase only control, have been proposed for the appropriate computation of the excitation coefficients, and several systems, especially in radar and astronomy applications, have been developed by research groups. X-band APAR (Active Phased Array Radar) [6], and HF/VHF-band RIAS (Radar a Impulsion et Antenne Synthetique) [7, 8], are two of the most recent non-mechanically antenna steering systems that are under testing. In the majority of the phased array systems that have been developed and tested, beamforming processing takes place at the RF stage. Beamforming at the IF stage, appears to be a lower cost solution.

Additionally, in some antenna applications, planar arrays have limitations imposed by the geometry of the design or the need for introducing an aerodynamic radome. If array elements are allocated over a conformal surface, those limitations may disappear. Cylindrical arrays, the most common type of conformal arrays, find applications in situations where wide scanning angles in azimuth are needed, exploiting their azimuth symmetry [9]. This benefit has found applications in broadcast antenna and direction finding antenna systems [10]. Cylindrical arrays usually require commutation [11, 12] of an illuminated region around the array. Practical surveillance and communication systems with azimuth scan requirements of 360 deg use cylindrical array geometries, but only a restricted sector of the cylinder illuminated. The illumination is commutated around the cylinder by means of switching network. A few examples of experimental cylindrical arrays that were designed and tested in the 70s are given here: In 1970, Boyns designed a ring array of 128 sectoral horns that it was fed by a parallel plate circular lens [13]. In 1970 too, Gabriel and Cummings introduced an L-band ring array that used two rings of 124 elements each, with 30 excited to form a beam. Elements were probe fed flared horns with chokes to reduce ring-to-ring coupling. This 20 ft diameter array used an elaborate switching and phasing unit [13].

In 1972, Provencher reviewed ring array practice with a cylindrical array with 256 elements in 32 columns. Each column of 8 dipoles incorporated a serpentine feed for frequency scanning in elevation. The switch matrix utilized 8 active columns, and provided an amplitude taper for 25 dB sidelobe level [13]. Finally, in 1976, Hannan tested an edge slot Doppler scan Microwave Landing System array in which each column was excited by a phaser [13].

2. EXPERIMENTAL PHASED ARRAY ANTENNA SYSTEM

In Figure 1, a block diagram of the experimental Phased Array Antenna System is presented. As it can be observed, it is organized in three units: the Beamforming Unit, the Transceivers Unit and the Antenna Array Unit.

Intermediate frequency input signal is divided through the IF Power Splitter to 11 individual IF signals which are phase adjusted through the Beamforming Unit. IF phase adjusted signals are inserted in parallel to the 11 TxRx modules of the Transceivers Unit, where they are upconverted, filtered and amplified. The microwave signals are finally emitted by the 21-element Antenna Array Unit at 10 GHz

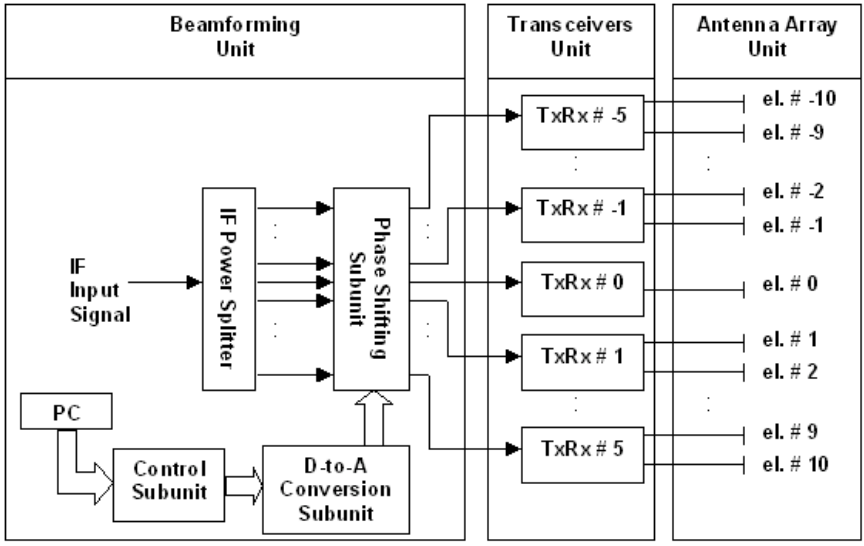

Figure 1. Experimental Phased Array Antenna System block diagram.

region. Every two successive antenna elements are fed by the same TxRx module, with the exception of the central one, which is driven by a single TxRx module.

2.1. Antenna Array Unit

The antenna of the system, originally designed in the framework of Western European Armament Group (WEAG)-THALES JP1.03-WEAG program [14–16], is a conformal array antenna consisting of a series of 21 microstrip patch elements. It is printed on the dielectric substrate Teflon RO4003, with electrical characteristics $\varepsilon_r = 3.38$, $\tan\delta = 0.0018$ and thickness $h = 0.51\,\text{mm}$. The whole structure is mounted on a cylindrical aluminum surface with radius of curvature 0.5 m, which gives the conformal feature to the system. Radiators are fed through coaxial probes, which run through aluminum surface and dielectric substrate, and touch the surface of each radiator. In Figure 2, the Antenna Array Unit is presented.

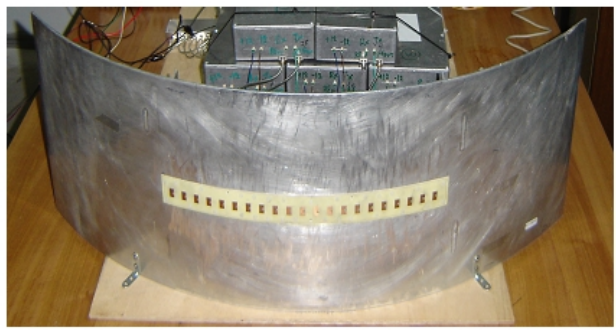

Figure 2. The Antenna Array Unit.

The 21 microstrip patch elements, numbered from −10 to 10 (el. # −10, el. # −9, ..., el. # −1, el. # 0, el. # 1ld el. # 9, el. # 10), are of rectangular shape, with dimensions 11 × 7 mm. Angular distance between adjacent elements is 2.27°, which corresponds to a $0.66 \times \lambda_0$ centre-to-centre distance. λ_0 is the free space wavelength at the 10 GHz operation frequency. As been placed on the cylinder, rectangular radiators follow its surface, having a 0.8° curvature.

Insertion loss at the input of each antenna element is given in Table 1 that follows.

Mutual coupling between each pair of successive antenna elements is given in Table 2 that follows. Values can be considered to be low enough so individual element's radiation is not affected by its adjacent

Table 1. Insertion Loss at the input of the antenna elements.

Antenna element	S_{11} (dB)	Antenna element	S_{11} (dB)
el. # -10	-15	el. # 1	-15
el. # -9	-17.3	el. # 2	-16
el. # -8	-17.1	el. # 3	-17
el. # -7	-18.2	el. # 4	-12.7
el. # -6	-15	el. # 5	-16.6
el. # -5	-16.3	el. # 6	-16.6
el. # -4	-12.5	el. # 7	-15
el. # -3	-17.2	el. # 8	-16.8
el. # -2	-11.2	el. # 9	-13.3
el. # -1	-17.6	el. # 10	-11.2
el. # 0	-18.1		

Table 2. Mutual Coupling between successive antenna elements.

Pair of successive antenna elements	S_{12} (dB)	Pair of successive antenna elements	S_{12} (dB)
el. # -10 / el. # -9	-23.4	el. # 0 / el. # 1	-25
el. # -9 / el. # -8	-24.1	el. # 1 / el. # 2	-24
el. # -8 / el. # -7	-24	el. # 2 / el. # 3	-24.2
el. # -7 / el. # -6	-24.3	el. # 3 / el. # 4	-25.2
el. # -6 / el. # -5	-24	el. # 4 / el. # 5	-25
el. # -5 / el. # -4	-24.2	el. # 5 / el. # 6	-24
el. # -4 / el. # -3	-23.8	el. # 6 / el. # 7	-23.5
el. # -3 / el. # -2	-24.2	el. # 7 / el. # 8	-23
el. # -2 / el. # -1	-23.9	el. # 8 / el. # 9	-24
el. # -1 / el. # 0	-25.4	el. # 9 / el. # 10	-24

elements.

As mentioned above, antenna elements are mounted on the surface of a cylinder of 0.5 m radius. In Figures 3a and 3b, two cases of individual element's simulated radiation patterns at H-pane are presented and the effect of conformality is discussed. In the first case, antenna element is placed on a planar surface, and in the second one it is placed on the cylinder. Agilent-HFSS 5.6 was used for the simulations.

Polar plots show that in case of the planar geometry, radiation peaks at the two directions $(\theta, \varphi) = (90°, \pm 24°)$, while radiation

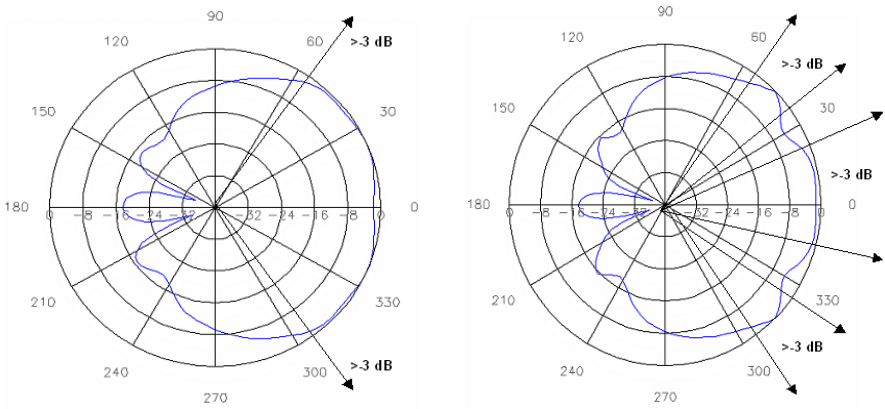

Figure 3. *H*-plane radiation pattern. (a) Antenna element is placed on a planar surface. (b) Antenna element is placed on a cylindrical surface.

intensity stays above -3 dB levels of its maximum value in the region $-60° \leftrightarrow 60°$. Outside of this region, radiated power is less than -3 dB level. In case of the cylindrical geometry, radiation peaks at two directions $(\theta, \varphi) = (90°, \pm 45°)$ which are wider compared to planar case. Additionally, in the region $-45° \leftrightarrow 45°$ the radiation intensity shown an oscillatory variation with respect to the -3 dB level. In the sectors $24° \leftrightarrow 36°$ and $-24° \leftrightarrow 36°$ it stays below the -3 dB level, while in sector $-24° \leftrightarrow 24°$ it is above of this level. Outside $-45° \leftrightarrow 45°$ region, radiation intensity drops monotonically below the level of -3 dB.

Comparing polar plots, it is obvious that cylindrical geometry influences the radiation patterns by spreading the power into wider sectors thus allowing wider angle operation of the phased array antenna.

2.2. Transceivers Unit

As block diagram of Figure 1 shows, the Transceivers Unit consists of 11 TxRx modules, numbered from -5 to 5 (TxRx # -5, TxRx # $-4, \ldots,$ TxRx # -1, TxRx # 0, TxRx # $1, \ldots,$ TxRx # 4, TxRx # 5). 11 IF signals, after been phase adjusted through the Beamforming Unit, are inserted one by one to these 11 modules at 140 MHz. After been filtered and upconverted at 1 GHz, they pass through the appropriate filters and been amplified. The final upconversion is at

10 GHz where signals are filtered again and been amplified by the final microwave amplifier. The 10 GHz amplified signal of each TxRx module enters into a power splitter where is divided to two 10 GHz signals which are finally connected to the radiators of the 21-element antenna array. This means that each two successive radiating elements are fed by the same TxRx module, with the exception of the central one (el. # 0), which is driven alone by a single module (TxRx # 0). This concept is also depicted in the block diagram of Figure 1.

In the receiver case, the 21 received signals are driven to the 11 TxRx modules following the same concept. They are amplified by the low noise amplifiers of the receiving chains, then filtered by suitable filters and finally downconverted to 1 GHz. The last step involves filtering, amplification and downconversion to 140 MHz.

In Figure 4, a TxRx module picture is shown. As duplexer unit a circulator (isolation 23 dB) is used to connect the transmitter and receiver to the antenna elements. During the transmission, the receiver channels are shut off in terms of dc supply. Through this, the isolation between the transmitter and receiver chains is approximately 100 dB.

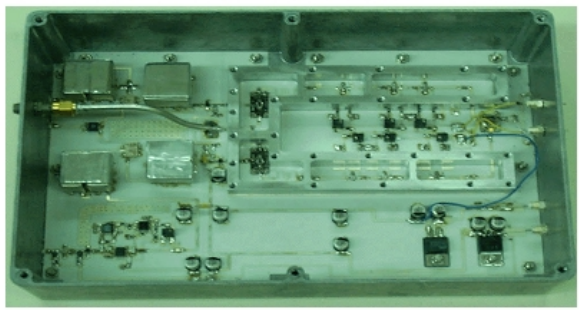

Figure 4. A TxRx module.

In order to generate the 1 GHz signals, a 900 MHz up/down conversion subunit has been designed and it is presented in Figure 5. The local oscillator is phase locked and has a phase noise at the order of −95 dBc at 100 kHz offset. Subunit provides 12 outputs of +13 dBm output power. The 11 of them are driven to the 11 TxRx modules, and the one remaining is terminated.

Finally, in order to generate the 10 GHz signals, a 9 GHz up/down conversion subunit has been designed. It consists of a 9 GHz local oscillator, a 9 GHz power amplifier and a 16-output RF power splitter. The local oscillator is phase locked while phase noise is at the order of −100 dBc at 100 KHz offset. Amplifier's output power is about 1 watt, while its gain is about 40 dB at 9 GHz. The 11 outputs of the power

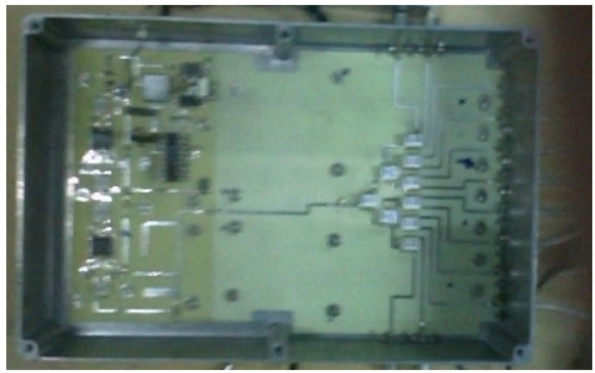

Figure 5. The 900 MHz up/down conversion subunit.

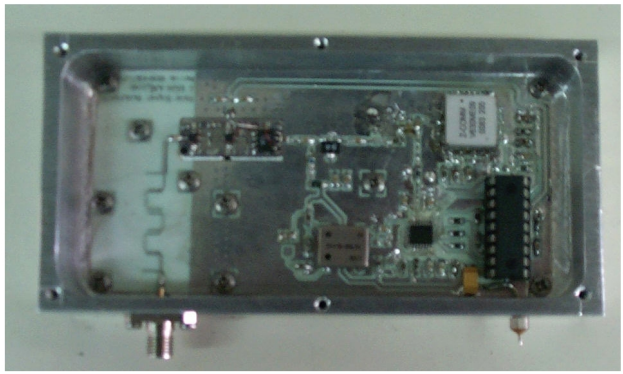

Figure 6. The 9 GHz local oscillator.

splitter are driven to the 11 TxRx modules, providing +15 dBm output power, while the 5 remaining ones are terminated. In Figures 6, 7 and 8, the three individual parts of the subunit are presented respectively.

2.3. Beamforming Unit

The Beamforming Unit is implemented at the IF stage. In a personal computer (PC), the operator of the system sets system's operation mode, scanning or non-scanning, defines the number of active radiators of the 21-element array antenna, and finally specifies the desired radiation pattern characteristics, i.e. main lobe and null directions. An operator's environment has been designed in ANCI-C code, using LabWindows-CVI environment of National Instruments. In Figure 9,

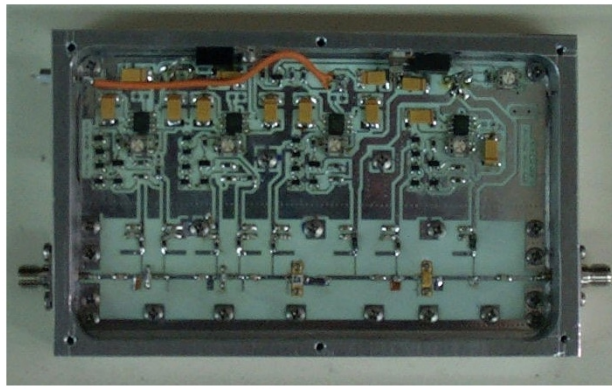

Figure 7. The 9 GHz power amplifier.

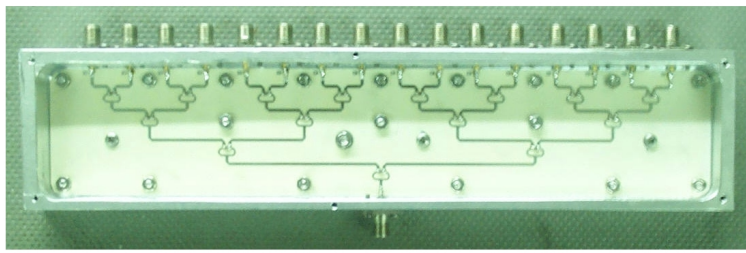

Figure 8. The 16-output 9 GHz power splitter.

operator-system communication windows are presented for several combinations of operation.

In **Operation Mode** field, operator selects system's operation mode, either non-scanning (*Normal*), Figures 9a and 9b, or scanning (*Scan*), Figures 9c and 9d. In the first case, desired main lobe's direction is set in **Direction (angle) F** field, while desired null's position is set in **Nulling Direction** field. In the second case, in **Direction (angle) F** and **Nulling Direction** fields, positions of scanning procedure initialization are set. Additionally, **Scan Step** and **Hop Delay (sec)** fields are activated and operator defines the scanning step in degrees and the time in seconds that radiation is focused on each discrete position respectively.

In # **of elements** field, operator sets the number of active radiators, *21* for total 21-element antenna array radiation, Figures 9a and 9c, or alternatively *7* for one out of three 7-element sectors radiation, Figures 9b and 9c. In that second case, **Sector** field is

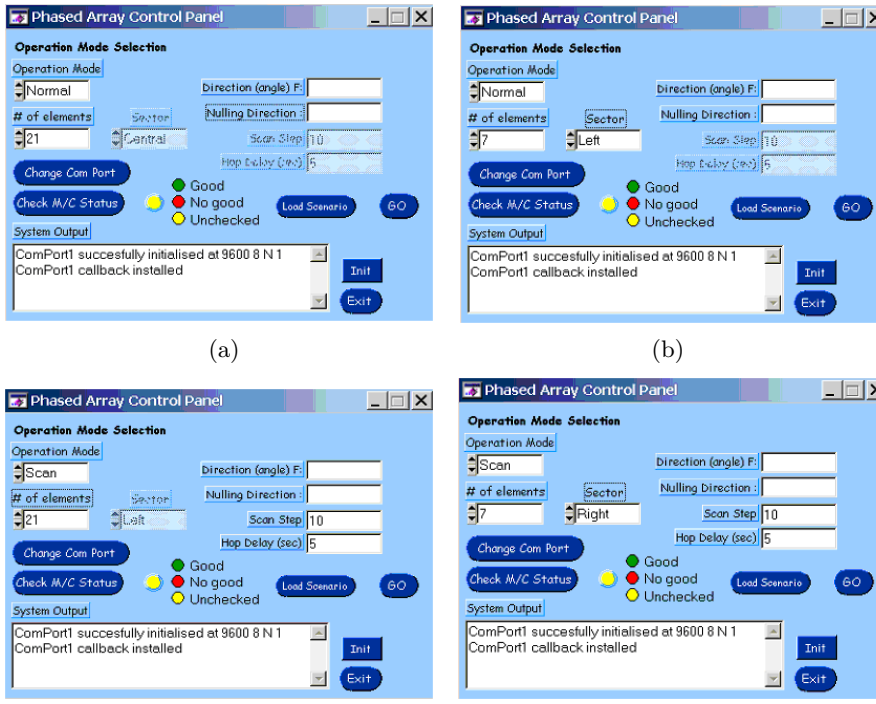

Figure 9. System operator's environment — 4 control cases.

activated where the desired 7-element sector, *Left, Center, Right*, is defined.

In **Change Com Port** field operator defines PC's serial port which will be used for data transmission. The Beamforming Unit's operation status can be checked through **Check M/C Status** command. **Init** command compensates phase offset among emitted signals according to the method that it will be presented in Section 4. By applying Load Scenario command, all specifications being set by the operator, are used to compute the appropriate phase shift values that must be set to the 11 IF signals. By applying **Go** command, digital data are sent to the subunits that follow next. In **System Output** field, the appropriate messages of proper operation or possible errors appear.

Phase shift values been computed based upon the specifications that operator sets, are transferred in digital form through an RS-232 serial interface to the Control Subunit, presented in Figure 10, where they are organized in 12-bit digital sequences. The appropriate control

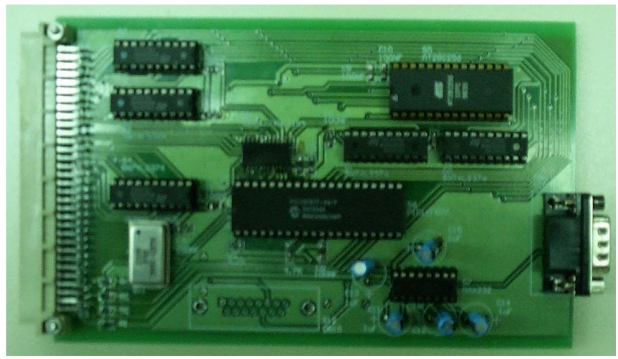

Figure 10. The Control Subunit.

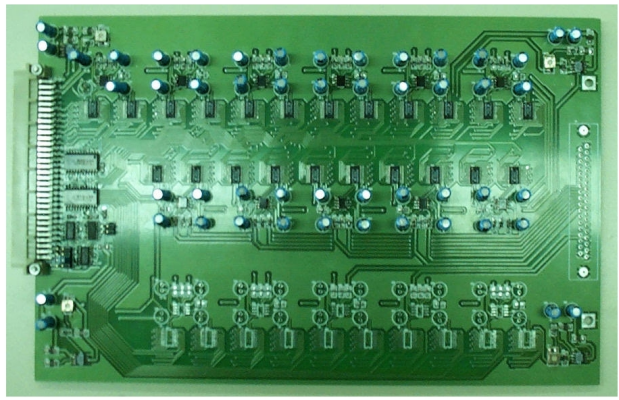

Figure 11. The Digital-to-Analog Conversion Subunit.

and synchronization signals are generated.

The 12-bit digital sequences are driven to the D-to-A Conversion Subunit, presented in Figure 11, where, under the guidance of control and synchronization signals, are converted to analog voltages, through Digital to Analog Converters (DACs). The range of each DAC output is 0–3 volt. DACs are characterized by 12-bit resolution and 1 μsec settling time. These features provide system high accuracy, as even extremely small phase shifts can be set, and high speed, as system can change its mode every 1 μsec. Additionally, DACs' outputs renew simultaneously, by the application of the appropriate common signal provided by the Control Subunit. So excitation phases are simultaneously updated at the inputs of the radiators. Each DAC is followed by an operational amplifier which upconverts DAC output

from 0–3 volt to 0–12 volt range.

These upconverted analog voltages are finally driven to the Phase Shifting Subunit where they control phase shifters setting the appropriate phase values. It consists of 11 channels, one for each of the 11 IF signals. Two phase shifters are connected in series in each IF channel, covering total $-180^\circ \leftrightarrow 180^\circ$ range. In Figure 12 that follows next, the Phase Shifting Subunit is presented.

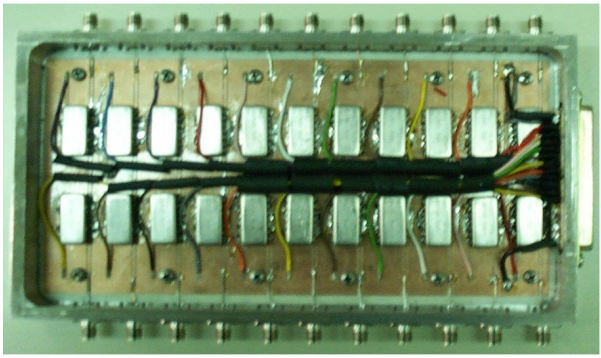

Figure 12. The Phase Shifting Subunit.

3. AMPLITUDES ADJUSTMENT

The Beamforming Unit computes and controls only the phases of the antenna element excitation currents to achieve the desired radiation patterns. This presupposes that amplitudes of the antenna element excitation currents should be constant. In Figure 13, it is observed that the amplitudes variation of the signals that are emitted by the 21 elements does not exceed ± 1 dB, so amplitudes can be considered to be constant.

4. PHASE CALIBRATION

The input signal at 140 MHz, till 21 antenna elements, passes through power divisions, amplifications and upconversions as well as suffers from cable differences in length. All these introduce phase offset among the 21 microwave signals that finally emitted at 10 GHz region. These phase offsets must be measured and be taken into account so as signals been phase adjusted correctly, according to the theoretically computed phase values.

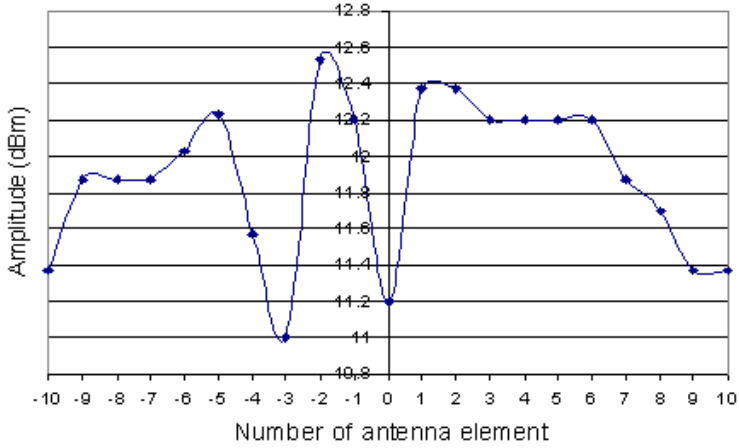

Figure 13. 21-element amplitudes of the excitation currents.

In this paper, phase calibration is implemented by the use of a "Magic T", based on its properties [17]. In Figure 14, an *E*-type "Magic T" is presented.

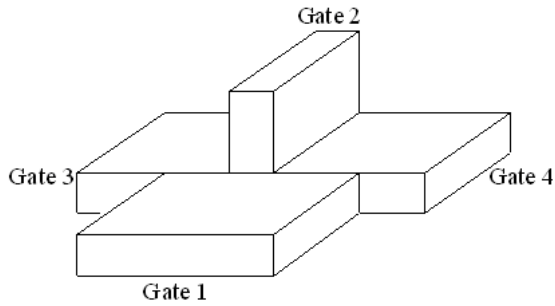

Figure 14. *E*-type "Magic T".

According to "Magic T" basic properties, if two in-phase signals insert to Gates 3 and 4 respectively, Gate 1 output signal will be maximized, while, simultaneously, Gate 2 output signal will be minimized. This aspect presupposes a minimum signal amplitudes variation and satisfactory matching at the inputs of the 'Magic T'. As presented in Figure 13, amplitude's variation does not exceed ± 1 dB, while reflection coefficients at the inputs of the experimental 'Magic T' that was used, are:

$$S_{11} = -17\,\text{dB}, \quad S_{22} = -10\,\text{dB}, \quad S_{33} = -20\,\text{dB}, \quad S_{44} = -17\,\text{dB}$$

These values can be considered to be low enough for the application.

Phase calibration procedure that is followed, is based on this property. Phase reference of the system (output of TxRx # 0) is connected to Gate 3. Gate 1 output, is driven to a spectrum analyzer and Gate 2 is terminated. Outputs of the rest of the 10 TxRx modules are driven successively to Gate 4. For each one of them, the corresponding phase shifters control voltages are manually changed, until power sign in the spectrum analyzer takes its maximum value. The two signals in Gates 3 & 4 are now inphase. Analog voltages are translated to the corresponding phase values, and phase offset between system reference (output of TxRx # 0) and each of the outputs of the rest of TxRx modules are calculated. In Figure 15, the measured phase offset between system's reference and each one of the TxRx modules outputs is given.

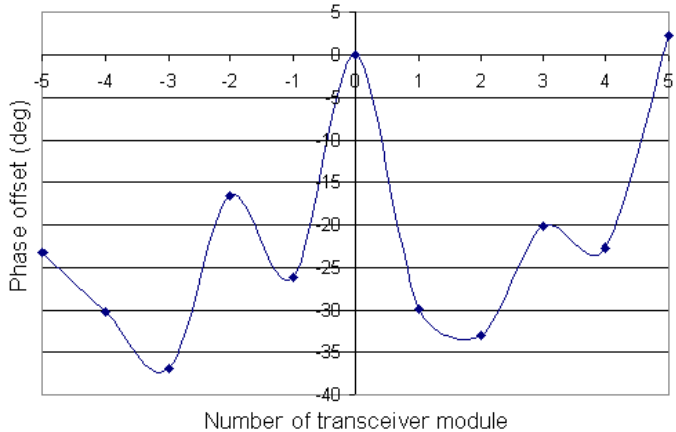

Figure 15. Phase offset between each TxRx module and phase reference (TxRx # 0).

5. RADIATION PATTERN SYNTHESIS & PHASE COMPUTATION

As the cylindrical array antenna in this paper consists of one series of 21 radiators, the achievement of desired radiation patterns can be considered as pattern synthesis on a circular arc array. Then the radiation is examined only at azimuth plane ($\theta = \pi/2$). The power intensity at azimuth plane of this arc array is expressed in the form

[18]:

$$U(\phi)=B\left|\sum_{n=-10}^{n=10} f(\phi+n\Delta\phi)\left|\overset{0}{\alpha}_n\right|\exp\left(j\frac{2\pi R}{\lambda}\left[[\cos(\phi-n\Delta\phi)]-\angle\overset{0}{\alpha}_n\right]\right)\right|^2 \tag{1}$$

where B is a normalization constant. $\Delta\varphi$ is the angular distance between adjacent elements, R is the radius of the cylinder and λ is the wavelength at the frequency of operation. In order to achieve the desired radiation pattern, the n-radiator's phase, $\angle\overset{0}{\alpha}_n$, must be appropriately set. It is reminded that amplitudes are taken to be constant which means:

$$\left|\overset{0}{\alpha}_{-10}\right|=\left|\overset{0}{\alpha}_{-9}\right|=\cdots=\left|\overset{0}{\alpha}_{-1}\right|=\left|\overset{0}{\alpha}_{0}\right|=\left|\overset{0}{\alpha}_{1}\right|=\cdots\left|\overset{0}{\alpha}_{9}\right|=\left|\overset{0}{\alpha}_{10}\right|=1 \tag{2}$$

In (1), $f(\phi+n\Delta\phi)$ is the antenna element pattern which, for the present conformal geometry is not separable from array factor and it is included in the sum. In case of a rectangular microstrip patch element, $f(\phi+n\Delta\phi)$ is given approximately by the expression [19]:

$$\begin{aligned} f(\phi+n\Delta\phi) \;=\; & C\cdot\cos(\phi+n\Delta\phi)\cdot\frac{\sin\left(\dfrac{kh\cdot\cos(\phi+n\Delta\phi)}{2}\right)}{\dfrac{kh\cdot\cos(\phi+n\Delta\phi)}{2}} \\ & \cdot\frac{\sin\left(\dfrac{kL\cdot\sin(\phi+n\Delta\phi)}{2}\right)}{\dfrac{kL\cdot\sin(\phi+n\Delta\phi)}{2}} \end{aligned} \tag{3}$$

where C is a normalization constant. h is the dielectric substrate thickness, L is the microstrip radiator's length and k is the wavelength number.

In order to compute the required antenna element excitation phases and to synthesize the desired radiation pattern, a least squares synthesis technique is applied. S. Prasad and R. Charan [20], utilized that approach for pattern synthesis of circular arc arrays with both phase and amplitude computation. In this paper, method is specialized synthesizing radiation patterns with phase computation only. According to this method [20], assuming a required power intensity pattern-mask $M(\varphi)$, a vector of phase excitations:

$$W^T=\left[\angle\overset{0}{\alpha}_{-10},\angle\overset{0}{\alpha}_{-9},\ldots,\angle\overset{0}{\alpha}_{-1},\angle\overset{0}{\alpha}_{0},\angle\overset{0}{\alpha}_{1},\ldots,\angle\overset{0}{\alpha}_{9},\angle\overset{0}{\alpha}_{10}\right] \tag{4}$$

is asked to be computed, which will produce a normalized power intensity pattern $U_0(\varphi)$, in a such way to minimize the mean square difference:

$$e^2 = \int |M(\phi) - U_0(\phi, \langle W \rangle)|^2 \cdot d\phi \tag{5}$$

It is convenient to consider the corresponding discretized problem where patterns are asked to be matched at a prespecified number of Π points, with Π sufficiently large. The problem can be set then as the minimization of the expression:

$$e^2 = \sum_{i=1}^{\Pi} |U_0(\phi_i, \langle W \rangle) - M(\phi_i)|^2 \tag{6}$$

The radiation pattern specifications are categorized on two classes. The first one contains system architecture con-straints. As it has already been mentioned and depicted in the block diagram of Figure 1, the 11 channels of the Phase Shifting Subunit drive one by one the 11 TxRx modules of the Transceivers Unit. Each TxRx module feeds every two successive radiators, with the exception of TxRx # 0 that feeds only one radiator, the central one (el. # 0). This means that each channel of the Phase Shifting Subunit adjusts the phase of every two adjacent radiators. The phase of the central radiator is adjusted alone by a single channel. According to this concept, phase values that are calculated using this technique must be equal for every two adjacent radiators, with the exception of the central one. In other words, computed phase values must satisfy the constraint:

$$\begin{array}{c} \angle \overset{0}{\alpha}_{-10} = \angle \overset{0}{\alpha}_{-9}, \angle \overset{0}{\alpha}_{-8} = \angle \overset{0}{\alpha}_{-7}, \ldots, \angle \overset{0}{\alpha}_{-2} = \angle \overset{0}{\alpha}_{-1}, \\ \angle \overset{0}{\alpha}_{1} = \angle \overset{0}{\alpha}_{2}, \angle \overset{0}{\alpha}_{3} = \angle \overset{0}{\alpha}_{4}, \ldots, \angle \overset{0}{\alpha}_{9} = \angle \overset{0}{\alpha}_{10} \end{array} \tag{7}$$

This constraint is of primary importance because technique must compute phase values that will be applicable to the experimental system that has been developed.

The second class of specifications contains the requirements of main lobe orientation, null positions and side lobes levels, and it is imposed by the appropriate selection of the pattern-mask $M(\varphi)$.

6. CALCULATED RESULTS

The calculated relative excitation phases, normalized to the phase reference of the system (el. # 0) and the corresponding calculated normalized radiation patterns for representative control cases, are now given. In each control case, the full line corresponds to the normalized radiation pattern and the doted one, to the given mask pattern.

6.1. Main Lobe at 0° - SLLs < -20 dB

In this case, main lobe is asked to be focused in the frontal direction, while side lobes must vary below -20 dB level. The calculated relative excitation phases are presented in the diagram of Figure 16.

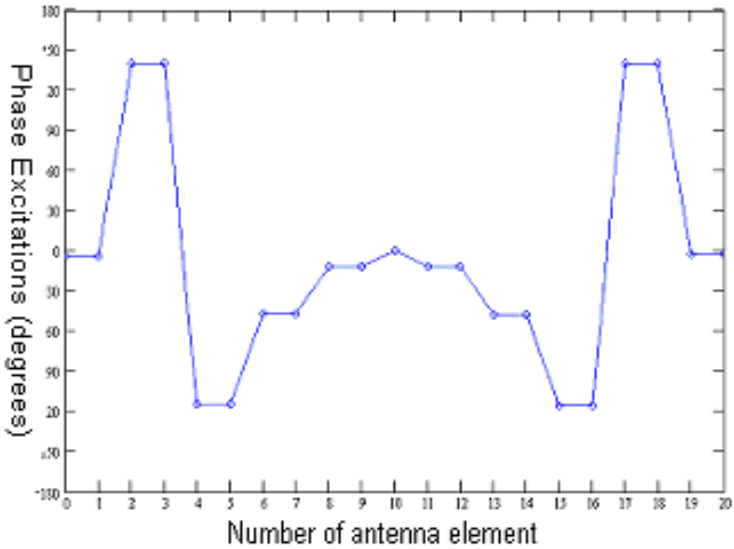

Figure 16. Normalized antenna element excitation phases. Main lobe at 0°, SLLs < -20 dB.

The normalized radiation pattern is given in Figure 17.

6.2. Main Lobe at 10° - Null at 16° - SLLs < -15 dB

Main lobe is now asked to be focused at 10°. A null is asked to be placed at 16°. Its depth must be -40 dB. Side lobe levels must vary below -15 dB. The calculated relative excitation phases for this control case are given in the diagram of Figure 18.

The corresponding normalized radiation pattern is given in Figure 19.

It is obvious that the first class of specifications, imposed by the architecture of the system is satisfied. Indeed, Figures 16 and 18 show that calculated phase excitations are equal for every two successive antenna elements, with the exception of the central one. This means that least squares synthesis technique that it was applied, provides applicable excitation currents for this experimental phased array antenna system.

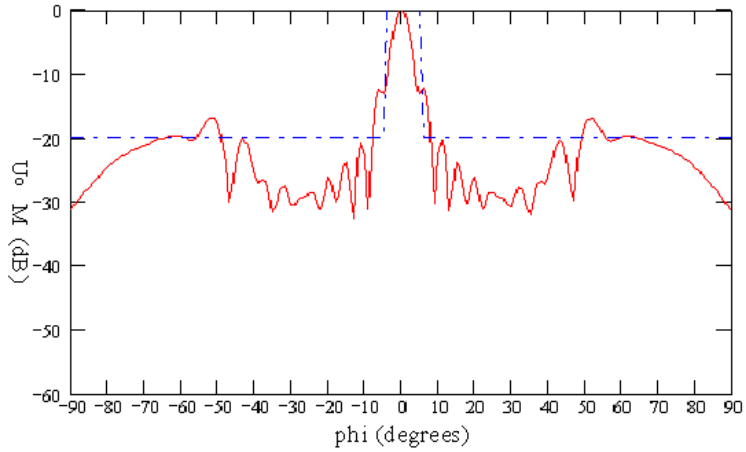

Figure 17. Calculated normalized radiation pattern and mask pattern. Main lobe at 0°, SLLs < -20 dB.

The corresponding calculated normalized radiation patterns that are presented in Figures 17 and 19 fulfill the specifications that mask pattern sets in terms of main lobe directions and nulls positions. Additionally, side lobes vary below levels that mask pattern sets in the azimuth range $-30° \leftrightarrow 30°$. Lower levels of side lobes can be achieved but this has consequences to the successive radiators phase equality constraint and method then provides non-applicable results to the system.

7. MEASURED RESULTS

In system's radiation pattern measurements, phase offset among different channels, was taken into account. Phase excitations W^T_{ADJ}, that were applied by the Beamforming Unit for each case that was examined is the sum of two factors:

$$W^T_{ADJ} = W^T - W^T_{CAL} \tag{8}$$

In (8), W^T is the vector of the phase excitations that are computed applying least squares synthesis for each case that was examined, and W^T_{CAL} is the vector of the phase offset values as it is given in Figure 15. It must be mentioned here that the phase offset between every two successive signals that are driven by the same TxRx module, is considered to be zero.

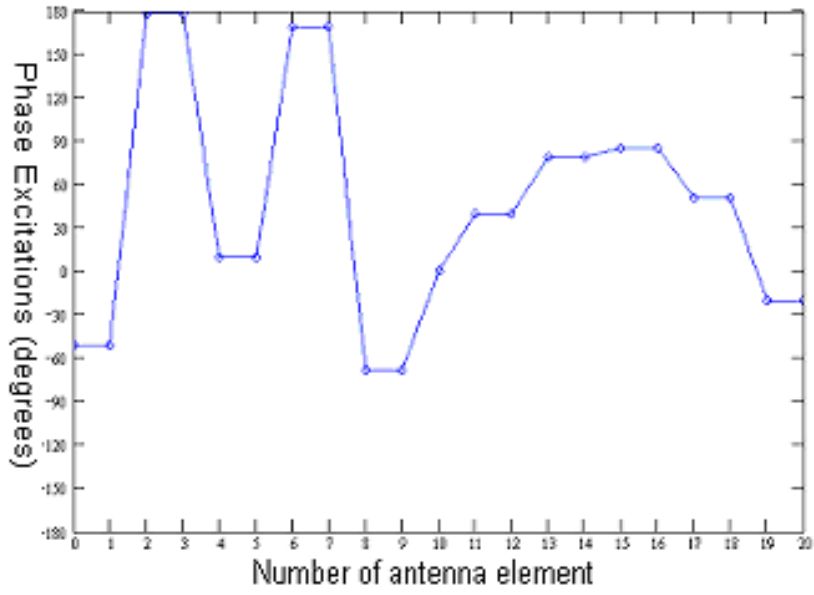

Figure 18. Normalized antenna element excitation phases. Main lobe at 10° - null at 16° - SLLs < -15 dB.

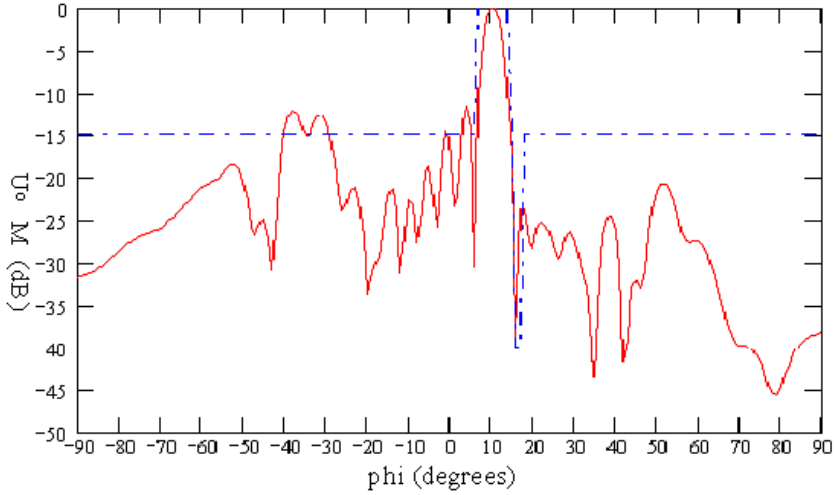

Figure 19. Calculated normalized radiation pattern and mask pattern. Main lobe at 10° - null at 16° - SLLs < -15 dB.

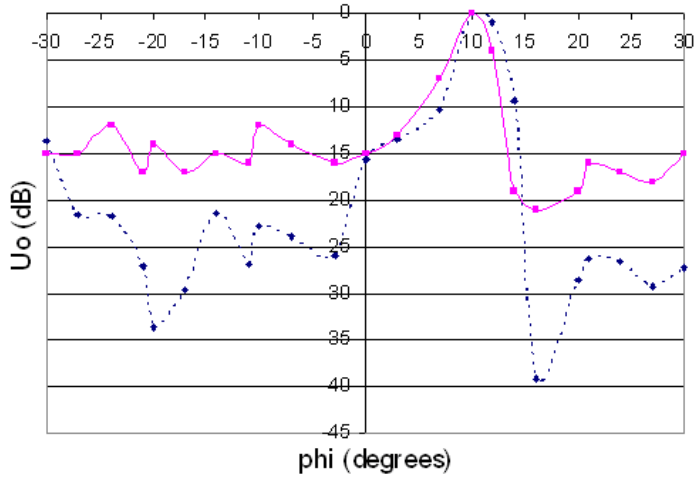

Figure 20. Normalized radiation pattern. Main lobe is at 0°. Full line corresponds to measurement while dotted line to calculation.

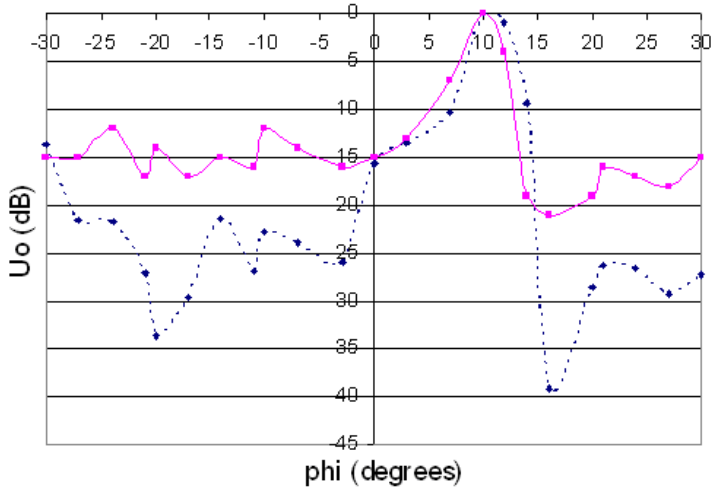

Figure 21. Normalized radiation pattern. Main lobe is at 10 and a null has been placed at 16°. Full line corresponds to measurement while dotted line to calculation.

In the following, radiation pattern measurements for the two control cases been examined in Section 6 are presented and been compared with calculated ones. Full lines correspond to the measured normalized radiation patterns whereas dotted ones correspond to calculated ones.

7.1. Main Lobe at 0°

From Figure 20 above, it is observed that measured radiation pattern has its maximum at 0° while side lobes are below −15 dB.

7.2. Main Lobe at 10° - Null at 16°

From Figure 21 it is observed that main lobe of the measured radiation pattern has been steered at 10°. A null has also been placed at 16°. Its depth is −21 dB. Side lobes vary below −12 dB.

8. CONCLUSION

An experimental phased array conformal (cylindrical) antenna system is presented in this paper. The use of IF processing to control the radiation pattern characteristics proved to be an approach providing stability and easy control of the radiation patterns as verified by the measurements and comparison with theoretical results, which shows good agreement. System provides radiation patterns with steerable main lobes and nulls at prespecified positions within the azimuth region $-30^\circ \leftrightarrow 30^\circ$ while its scanning speed is 8 μs. The possibility of using the developed conformal array as focal plane radiator in a large reflector antenna is an interesting application being considered.

REFERENCES

1. Skolnik, M. I., *Phased Array Antennas*, Artech House Inc., Norwood, 1972.
2. Ridenour, L. N., *Radar System Engineering*, McGraw-Hill Book Co., New York, 1947.
3. Smith, R. A., *Aerials for Metre and Decimetre Wavelengths*, Cambridge University Press, London, 1949.
4. Price, A., *Instruments of Darkness*, Charles Scribner's Sons, New York, 1970.
5. Stergiopoulos, S., *Advanced Signal Processing Handbook*, 1st ed., CRC Press, 2000.

6. Golshayan, A. K., S. V. D. Schoot, and P. Genderen, "Active Phases Array Radar (APAR)," *Proc. of the 5th International Conference on Radar Systems, Brest (F)*, 1999.
7. Dorey, J. and G. Garnier, "RIAS, Radar a Impulsion et Antenne Synthetique," *L' Onde Electrique*, Vol. 69, No. 6, 36–44, November–December 1989.
8. Luce, A.-S., H. Molina, D. Mulller, and V. Thirard, "Experimental results on RIAS digital beamforming radar," *Proc. of the International Conference Radar* 92, Brighton, UK, 1992.
9. Skolnik, M. I., *Introduction to Radar Systems*, 2nd ed., McGraw-Hill International Editions, New York, 1981.
10. Mailloux, R. J., *Phased Array Antenna Handbook*, 2nd ed., Artech House Publishers, Norwood, 1994.
11. Provincher, J., H., "A survey of circular symmetric arrays," *Proc. 1970 Phased Array Antenna Symp.*, Dedham, MA, June 1972.
12. Hill, R. J., *Phased Array Antennas*, Artech House, Dedham, MA, 1972.
13. Hansen, R. C., *Phased Array Antennas*, 2nd ed., John Wiley & Sons, Inc., New York, 1998.
14. Uzunoglu, N. K., D. I. Kaklamani, G. E. Stratakos, et al., "On the development of a conformal array system," *Workshop Cost-260*, Dubrovnik, Croatia, Dec. 1997.
15. Uzunoglu, N. K., D. I. Kaklamani, G. E. Stratakos, et al., "Design of a cylindrically shaped conformal array system," *28th European Microwave Conference*, Amsterdam, Nederland, 1998.
16. Koukourlis, C. S., G. A. Kyriacou, S. G. Mavrides, S. K. Diamantis, K. Th. Spyridakis, J. N. Sahalos, G. Stratakos, P. Tsenes, and N. Uzunoglou, "Design and development of an active printed cylindrical antenna array for radar applications," *Union Radio-Scientifique Internationale*, Maastricht, Nederland, Aug. 2002.
17. Marcuvitz, N., *Waveguide Handbook*, Dover Pub. Inc., New York, 1965.
18. Litva, J. and T. K.-Y. Lo, *Beamforming in Wireless Communications*, 1st ed., Artech House Publishers, Norwood, 1996.
19. Garg, R., P. Bhartia, I. Bahl, and A. Ittipiboon, *Microstrip Antenna Design Handbook*, 1st ed., Artech House, Inc., Norwood, 2001.
20. Prasad, S. and R. Charan, "On the constrained synthesis of array patterns with applications to circular and arc arrays," *IEEE Transactions on Antennas and Propagation*, Vol. AP-32, No. 7, 725–730, 1984.